Electronic Supplementary Information for

Ultralow thermal conductivity and thermally-deactivated electrical transport in a 1D silver array with alternating δ-bonds

Nahid Hassan,[a] Suneetha Nagaraja,[b] Sauvik Saha,[a] Kartick Tarafder,[b] and Nirmalya Ballav*[a]

[a]*Department of Chemistry, Indian Institute of Science Education and Research, Dr. Homi Bhabha Road, Pune – 411 008, India.*
[b]*Department of Physics, National Institute of Technology Karnataka, Surathkal, Mangalore – 575 025, India.*

***nballav@iiserpune.ac.in**

Experimental

Materials

Silver(I) bromide (AgBr; 99%), tetramethylammonium bromide (TMAB; ≥ 98 %) and hydrobromic acid (48 wt.% in H_2O; ≥ 99.99%) were purchased from Sigma-Aldrich. Acetone (HPLC grade), DMF (HPLC grade), DMSO (HPLC grade) and hypophosphorous acid (H_3PO_2; 50 wt.% in H_2O) were purchased from RANKEM (India). All chemicals were used without any further purification.

Synthesis of (TMA)$AgBr_2$ single crystals

Single crystals of (TMA)$AgBr_2$ is synthesized following a slow cooling process. Typically, 1 mmol TMAB (154.04 mg) and 1 mmol AgBr (187.77 mg) are taken in a glass vial. A mixed solvent of 4 mL DMF, 1 mL DMSO and 3 mL Acetone is then added to the vial, followed by the addition of 200 µL H_3PO_2 to prevent any areal oxidation. The resulting solution is sonicated and subsequently heated at 65 °C for 6 h to dissolve the reactants. Then the reaction mixture is filtered through a 0.22 µ syringe filter, and finally allowed to cool to room temperature naturally. Sharp needle like white crystals were yielded upon cooling. Crystals were further filtered, washed with acetone and dried in a vacuum oven at 100 °C for 12 h before additional characterization.

Characterization

Single crystals were taken for diffraction in a Bruker Smart Apex Duo diffractometer at 150 K, 298 K and 340 K using Mo Kα radiation (λ = 0.71073 Å). APEX4 software was used to do the absorption corrections. Crystal structure was solved by the direct method and refined by full-matrix least-squares on F2(SHELXL-2014/6) and Olex2 with ShelXT2 structure solution program.[1-3] Additional structural refinement data are presented in the Supplementary Information. PXRD patterns were recorded on a Bruker D8 Advance diffractometer with Cu Kα radiation (λ = 1.5406 Å). XPS spectra were recorded by using a Thermo Kalpha+ spectrometer equipped with micro-focused and monochromated AlKα radiation. TGA profiles were recorded using Perkin-Elmer thermal analyzer STA 6000 model. Differential Scanning Calorimetry (DSC) measurements were done using TA Q20 differential scanning calorimeter. Thermal diffusivity measurements were carried out on Linses LFA 1000. Solid-state UV-vis spectra were recorded on Shimadzu UV-vis-

NIR spectrophotometer (Model UV-3600 plus). Electrical transport measurements on pelletized samples were carried out using a Keithley 4200 SCS Parameter Analyzer system assembled with an Everbeing probe station using Au-plated W-tip as micro-contact electrodes. Raman spectra (λ_{exc} = 632.8 nm) were recorded at Raman microscope (LabRAM HR, HoribaJobinYvon) using a 50x objective lens (spectral resolution of the system is ~1 cm^{-1}).

Computational details

The structure is optimized and electronic properties are calculated using the density functional theory as implemented in the Vienna Abintio Simulation Package (VASP).[4] The Energy convergence criteria is set to 10^{-5} eV and the accuracy of force convergence on all atoms is set to 0.01 eV A^{-1}. A conjugate gradient algorithm is used to relax the ions into their instantaneous ground states. The brilliouin zone sampling is done using the Gamma only k-point grid with k-point mesh of 4x3x2. The Gaussian smearing method with smearing width 0.05 eV is used to optimize the orbitals. The generalized gradient approximation (GGA) exchange correlation is used to optimize the structure as suggested by Perdew, Burke and Ernzerhof (PBE). The on-site Coulomb interaction due to the 4d electrons has been taken into account using the DFT+U method with an effective U value of 5.8 eV and the value of U-J is 5.8 eV (J=0).[5] The Projected and the total density of states are obtained from the optimized structure.

Table S1. Crystal data and structure refinement for the (TMA)$AgBr_2$ system (150 K).

Empirical formula	C4 H12 Ag Br2 N	
Formula weight	341.84	
Temperature	150(2) K	
Wavelength	MoKα (λ = 0.71073 Å)	
Crystal system	Orthorhombic	
Space group	I m m m	
Unit cell dimensions	a = 6.7744(13) Å	α= 90°.
	b = 9.1274(19) Å	β= 90°.
	c = 15.003(3) Å	γ= 90°.
Volume	927.7(3) $Å^3$	
Z	4	
Density (calculated)	2.448 g/cm^3	
Absorption coefficient	10.708 mm^{-1}	
F(000)	640	
Crystal size	0.681 x 0.119 x 0.044 mm^3	
Theta range for data collection	2.612 to 25.361°.	
Index ranges	$-7 \leq h \leq 8$, $-10 \leq k \leq 10$, $-17 \leq l \leq 18$	
Reflections collected	4058	
Independent reflections	512 [R(int) = 0.0580]	
Completeness to theta = 25.242°	99.4 %	
Absorption correction	Semi-empirical from equivalents	
Max. and min. transmission	0.7452 and 0.3149	
Refinement method	Full-matrix least-squares on F^2	
Data / restraints / parameters	512 / 9 / 31	
Goodness-of-fit on F^2	1.107	
Final R indices [I>2sigma(I)]	R1 = 0.0769, wR2 = 0.1817	
R indices (all data)	R1 = 0.0800, wR2 = 0.1837	
Extinction coefficient	n/a	
Largest diff. peak and hole	1.692 and -3.345 $e.Å^{-3}$	

Table S2. Atomic Coordinates (x 10^4) and equivalent isotropic displacement parameters ($Å^2$ x 10^3) for the (TMA)$AgBr_2$ single crystal (150 K).

U(eq) is defined as one third of the trace of the orthogonalized U^{ij} tensor.

	x	y	z	U(eq)
Ag(1)	7326(3)	5000	5000	29(1)
Br(1)	10000	5000	6368(2)	26(1)
Br(2)	5000	2609(4)	5000	31(1)
N(1)	5000	5000	8027(16)	25(5)
C(1)	5000	3680(20)	7419(15)	33(4)
C(2)	6810(40)	5000	8615(17)	55(7)

Table S3. Bond lengths and bond angles in the (TMA)$AgBr_2$ single crystal (150 K).

	Length/Å
Ag(1)-Br(2)	2.692(3)
Ag(1)-Br(2)#1	2.692(3)
Ag(1)-Br(1)	2.738(3)
Ag(1)-Br(1)#2	2.738(3)
Ag(1)-Ag(1)#1	3.152(5)
N(1)-C(1)	1.51(3)
N(1)-C(1)#3	1.51(3)
N(1)-C(2)	1.51(3)
N(1)-C(2)#3	1.51(3)
	Angle/°
Br(2)-Ag(1)-Br(2)#1	108.34(11)
Br(2)-Ag(1)-Br(1)	112.79(3)
Br(2)#1-Ag(1)-Br(1)	112.79(3)
Br(2)-Ag(1)-Br(1)#2	112.79(3)
Br(2)#1-Ag(1)-Br(1)#2	112.79(3)
Br(1)-Ag(1)-Br(1)#2	97.14(10)
Br(2)-Ag(1)-Ag(1)#1	54.17(6)
Br(2)#1-Ag(1)-Ag(1)#1	54.17(6)
Br(1)-Ag(1)-Ag(1)#1	131.43(5)
Br(1)#2-Ag(1)-Ag(1)#1	131.43(5)
Ag(1)#2-Br(1)-Ag(1)	82.86(10)
Ag(1)-Br(2)-Ag(1)#1	71.66(11)
C(1)-N(1)-C(1)#3	106(2)
C(1)-N(1)-C(2)	110.7(7)
C(1)#3-N(1)-C(2)	110.7(7)
C(1)-N(1)-C(2)#3	110.7(7)
C(1)#3-N(1)-C(2)#3	110.7(7)
C(2)-N(1)-C(2)#3	109(3)

Symmetry transformations used to generate equivalent atoms:

#1 -x+1,-y+1,-z+1 #2 -x+2,-y+1,-z+1 #3 -x+1,-y+1,z

Table S4. Crystal data and structure refinement for the (TMA)$AgBr_2$ system (298 K).

Empirical formula	C4 H12 Ag Br2 N	
Formula weight	341.84	
Temperature	298(2) K	
Wavelength	0.71073 Å	
Crystal system	Orthorhombic	
Space group	I m m m	
Unit cell dimensions	a = 6.7923(10) Å	a= 90°.
	b = 9.1285(16) Å	b= 90°.
	c = 15.017(2) Å	g = 90°.
Volume	931.1(2) $Å^3$	
Z	4	
Density (calculated)	2.439 g/cm^3	
Absorption coefficient	10.668 mm^{-1}	
F(000)	640	
Crystal size	0.437 x 0.117 x 0.074 mm^3	
Theta range for data collection	3.292 to 24.673°.	
Index ranges	-7<=h<=7, -10<=k<=10, -17<=l<=17	
Reflections collected	3750	
Independent reflections	475 [R(int) = 0.0429]	
Completeness to theta = 24.673°	99.6 %	
Absorption correction	Semi-empirical from equivalents	
Max. and min. transmission	0.7451 and 0.4357	
Refinement method	Full-matrix least-squares on F^2	
Data / restraints / parameters	475 / 6 / 32	
Goodness-of-fit on F^2	1.085	
Final R indices [I>2sigma(I)]	R1 = 0.0234, wR2 = 0.0445	
R indices (all data)	R1 = 0.0260, wR2 = 0.0454	
Extinction coefficient	0.0027(3)	
Largest diff. peak and hole	0.486 and -0.466 $e.Å^{-3}$	

Table S5. Crystal data and structure refinement for the (TMA)$AgBr_2$ system (340 K).

Empirical formula	C4 H12 Ag Br2 N	
Formula weight	341.84	
Temperature	340(2) K	
Wavelength	0.71073 Å	
Crystal system	Orthorhombic	
Space group	I m m m	
Unit cell dimensions	a = 6.797(3) Å	a= 90°.
	b = 9.193(5) Å	b= 90°.
	c = 15.120(7) Å	g = 90°.
Volume	944.8(8) $Å^3$	
Z	4	
Density (calculated)	2.403 g/cm^3	
Absorption coefficient	10.514 mm^{-1}	
F(000)	640	
Crystal size	0.498 x 0.098 x 0.078 mm^3	
Theta range for data collection	2.593 to 25.006°.	
Index ranges	-7<=h<=8, -10<=k<=10, -17<=l<=17	
Reflections collected	5184	
Independent reflections	500 [R(int) = 0.0974]	
Completeness to theta = 25.006°	99.2 %	
Absorption correction	Semi-empirical from equivalents	
Max. and min. transmission	0.0971 and 0.0213	
Refinement method	Full-matrix least-squares on F^2	
Data / restraints / parameters	500 / 0 / 31	
Goodness-of-fit on F^2	1.147	
Final R indices [I>2sigma(I)]	R1 = 0.0893, wR2 = 0.2333	
R indices (all data)	R1 = 0.1083, wR2 = 0.2576	
Extinction coefficient	n/a	
Largest diff. peak and hole	1.663 and -2.205 $e.Å^{-3}$	

Table S6. Variable temperature SCXRD parameters of (TMA)$AgBr_2$ single crystal.

Temperature	150 K	298 K	340 K
a (Å)	6.7744(13)	6.7923(10)	6.797(3)
b (Å)	9.1274(19)	9.1285(16)	9.193(5)
c (Å)	15.003(3)	15.017(2)	15.120(7)
α (°)	90	90	90
β (°)	90	90	90
γ (°)	90	90	90
Space Group	Immm	Immm	Immm

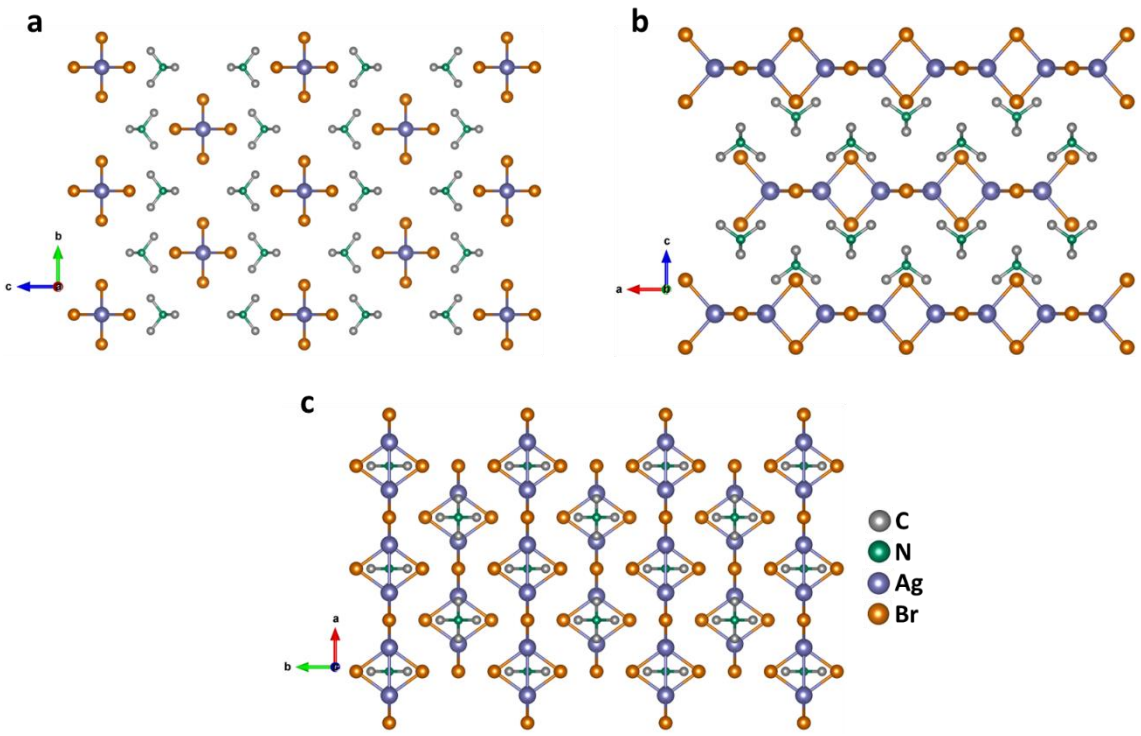

Figure S1. Crystal structure of (TMA)$AgBr_2$ viewed along (a) a-axis, (b) b-axis, and (c) c-axis. H atoms are omitted for clarity. Each $(AgBr_2)_n^{n-}$ inorganic chain is surrounded by six stacks of TMA^+ cations.

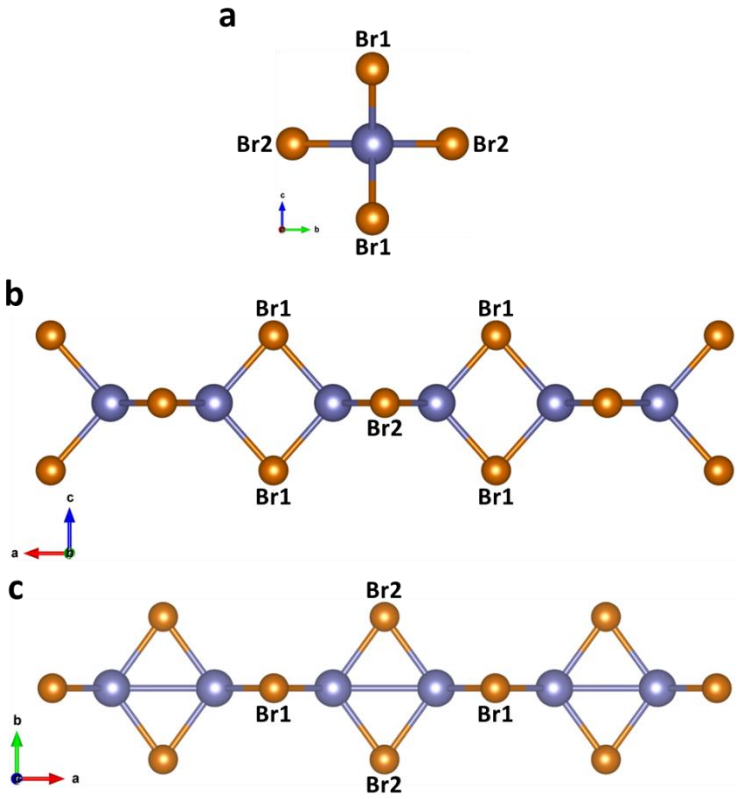

Figure S2. Polymeric chain of $(AgBr_2)_n^{n-}$ anions viewed along (a) a-axis, (b) b-axis and (c) c-axis. Silver and bromine atoms are represented by purple, and brown coloured spheres.

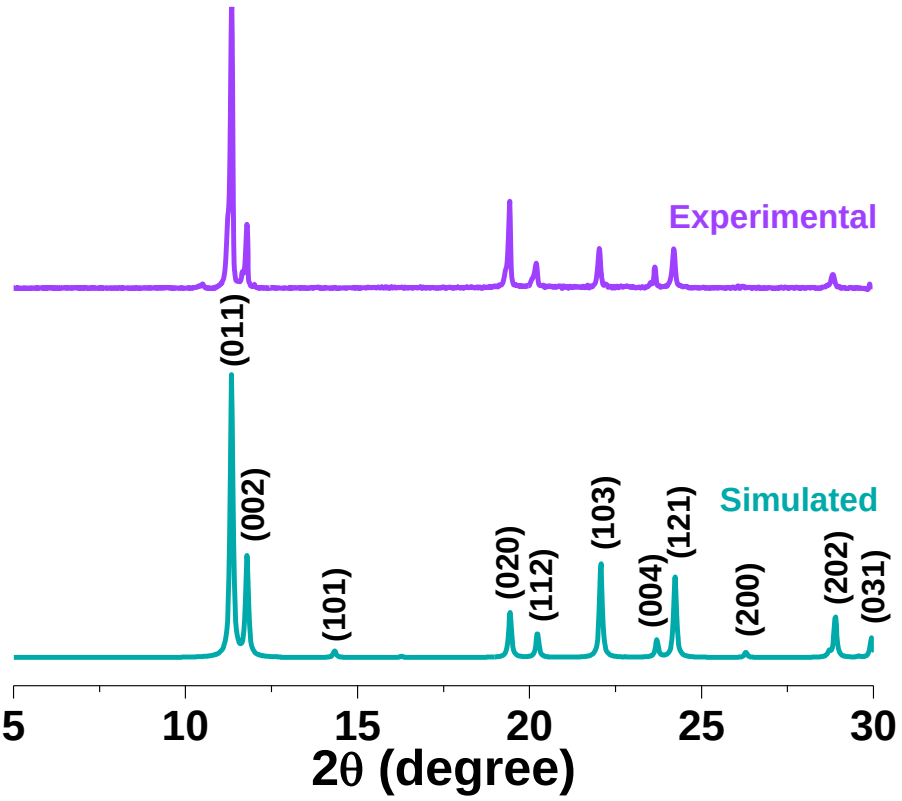

Figure S3. Comparison between the simulated and experimental PXRD patterns showing phase purity of (TMA)$AgBr_2$.

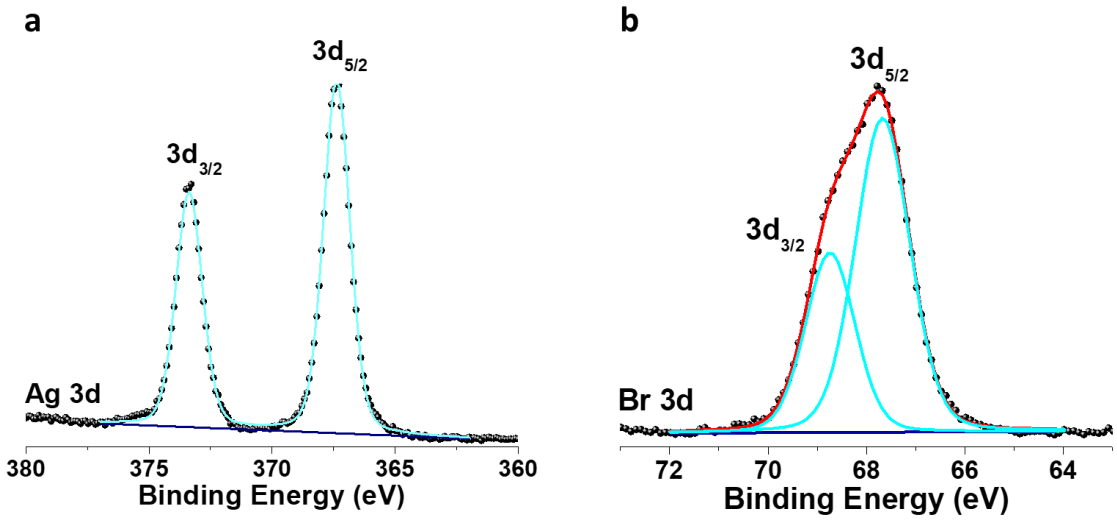

Figure S4. (a) Ag3d XPS spectrum featuring spin-orbit coupled (~6.0 eV) doublet signals ($3d_{5/2}$ and $3d_{3/2}$). Raw spectral data points (black spheres) were duly fitted (red lines). (b) Br3d XPS spectrum featuring spin-orbit coupled (~1.05 eV) doublet signals ($3d_{5/2}$ and $3d_{3/2}$). Raw spectral data points (black spheres) were duly fitted (red lines).

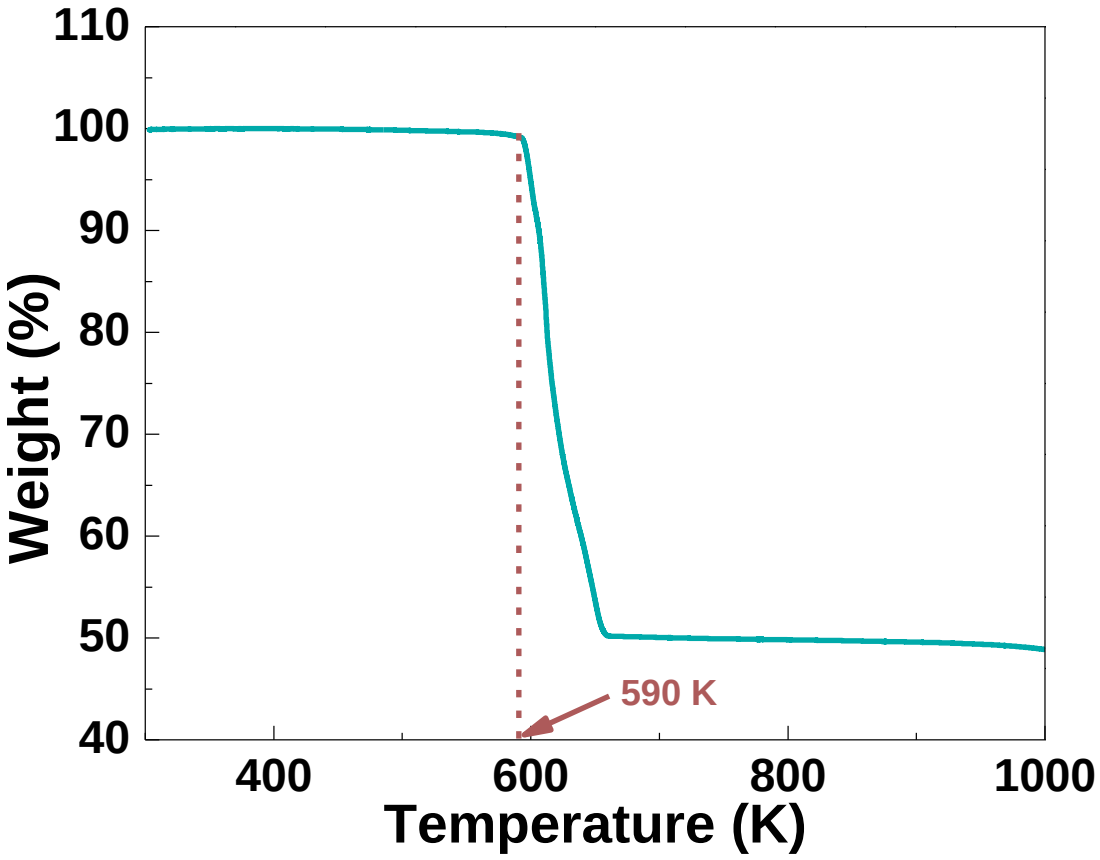

Figure S5. Thermogravimetric analysis (TGA) of (TMA)$AgBr_2$ indicating excellent thermal stability up to ~600 K.

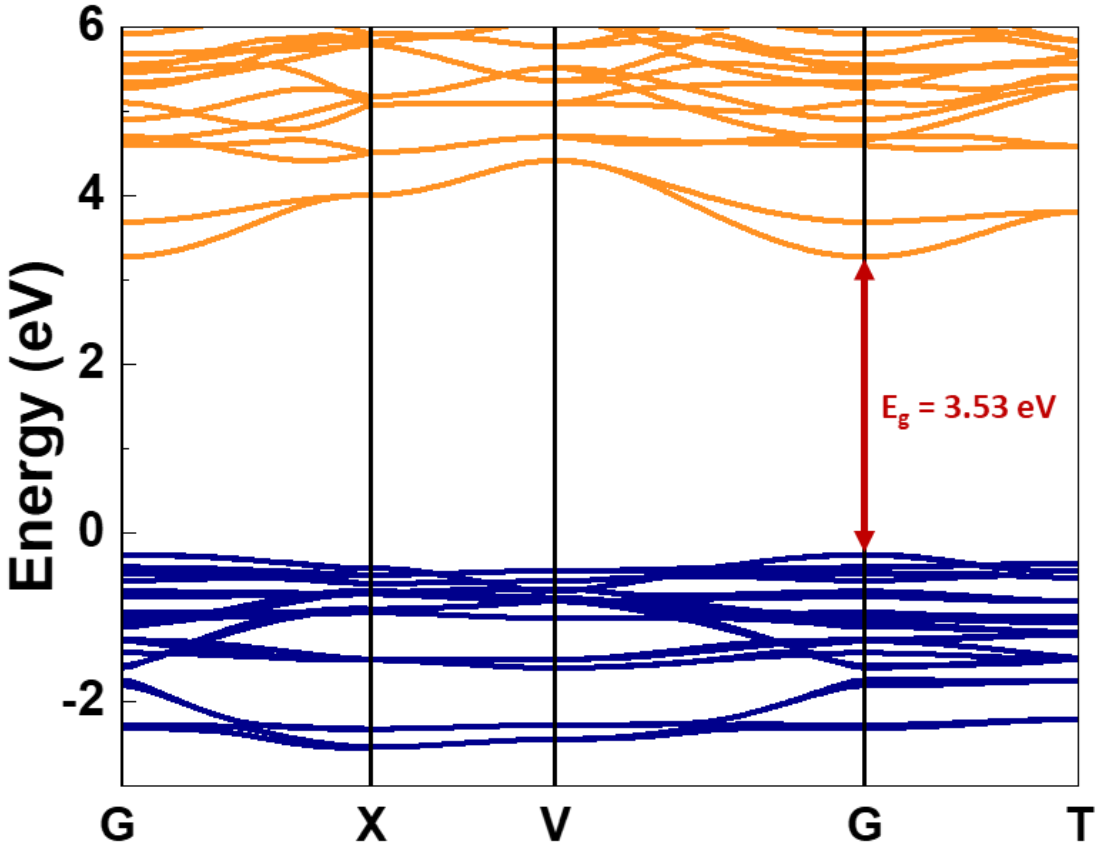

Figure S6. Electronic band structure calculated from density functional theory showing direct bandgap (E_g) value of 3.53 eV at the Gamma (G) point.

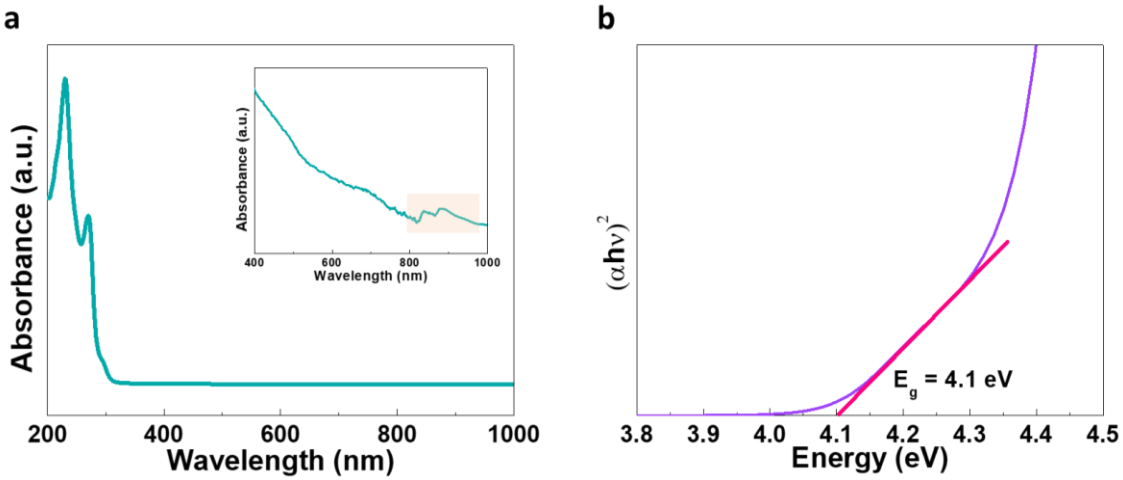

Figure S7. (a) Room temperature solid-state UV-visible absorption (DRS) spectrum of (TMA)$AgBr_2$ (inset: zoomed-in regions with finite absorption features at higher wavelengths). (b) Tauc plot of (TMA)$AgBr_2$ showing the experimental band gap.

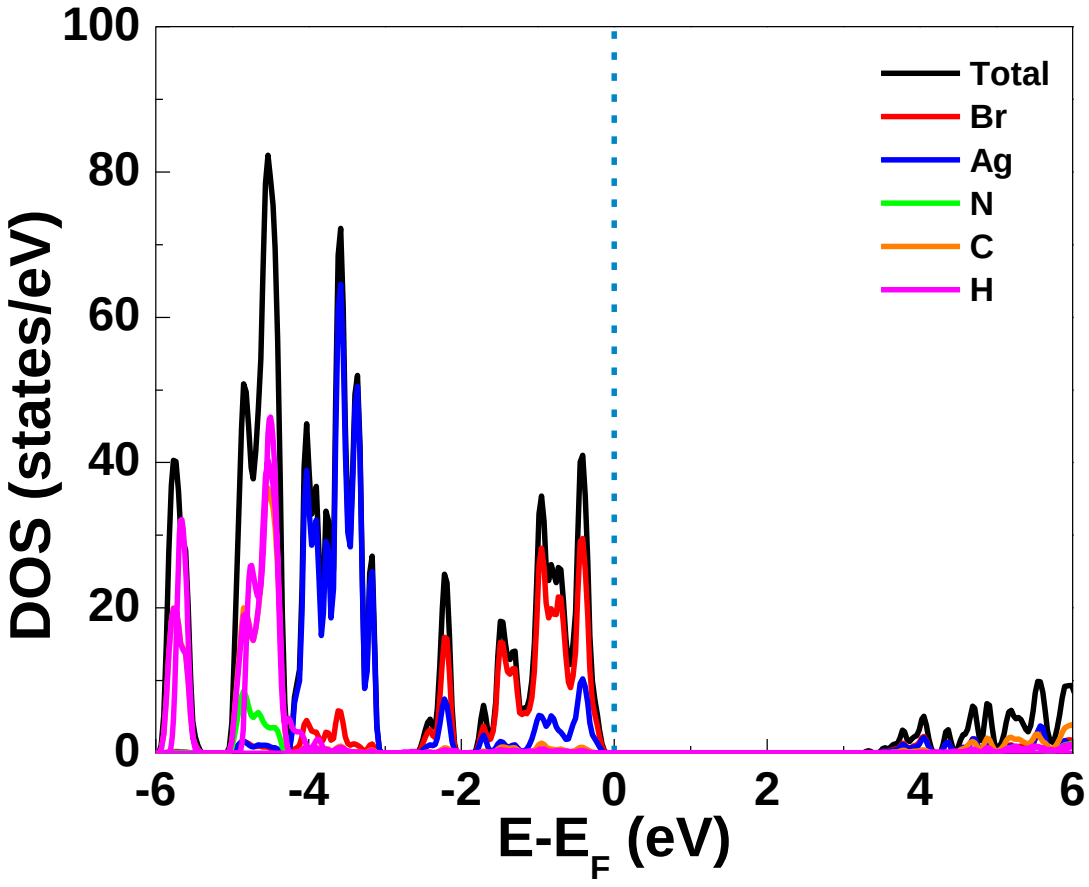

Figure S8. Density of states (DOS) plots exhibiting the total as well as atomic contributions. Dotted vertical line represents the Fermi level (E_F).

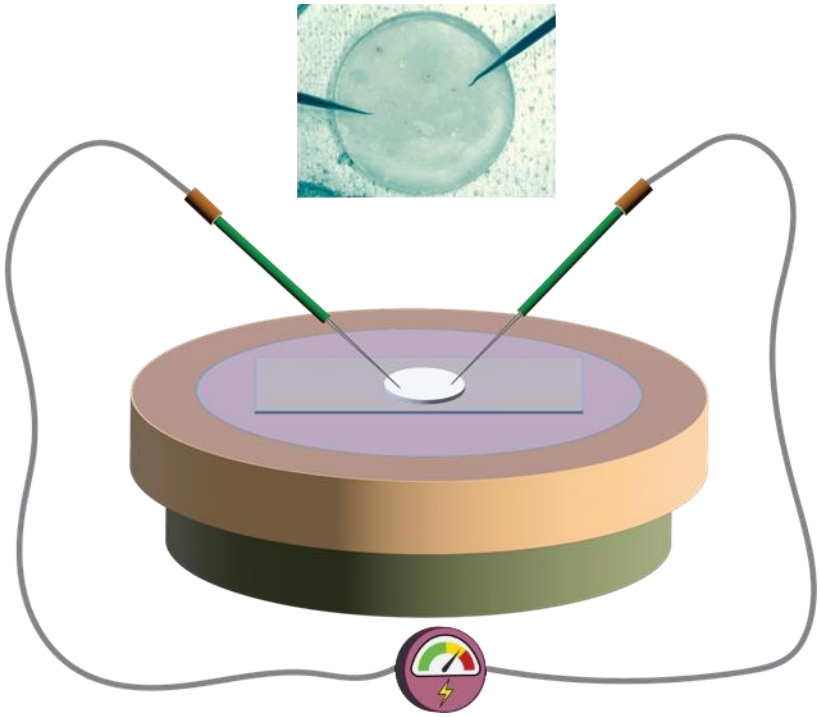

Figure S9. Schematic diagram of the device for two probe measurements of current-voltage (*I*-*V*) properties. Inset shows optical image of the real two probe set-up with contact electrodes.

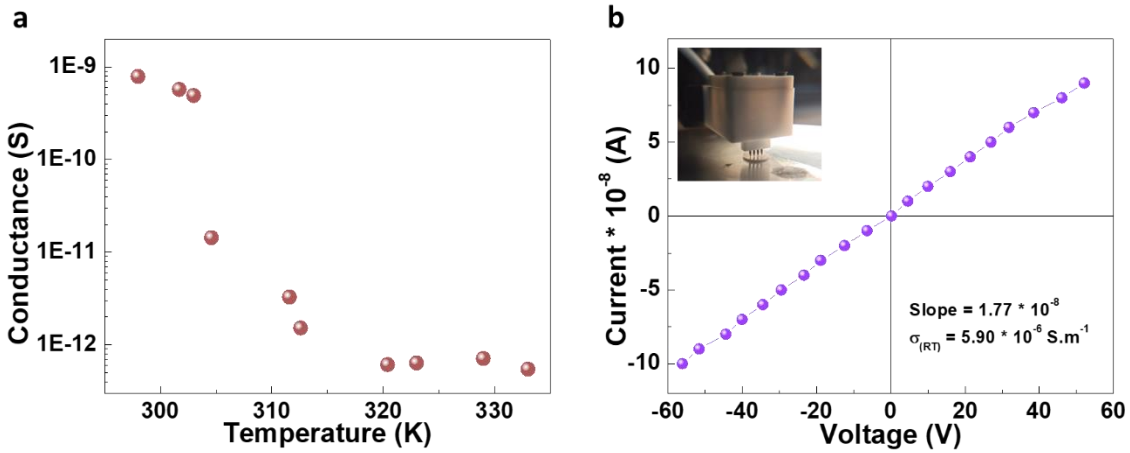

Figure S10. (a) Electrical conductance of (TMA)$AgBr_2$ as a function of temperature. (b) Room temperature electrical conductivity using colinear four probe set-up. Inset shows the real four probe device.

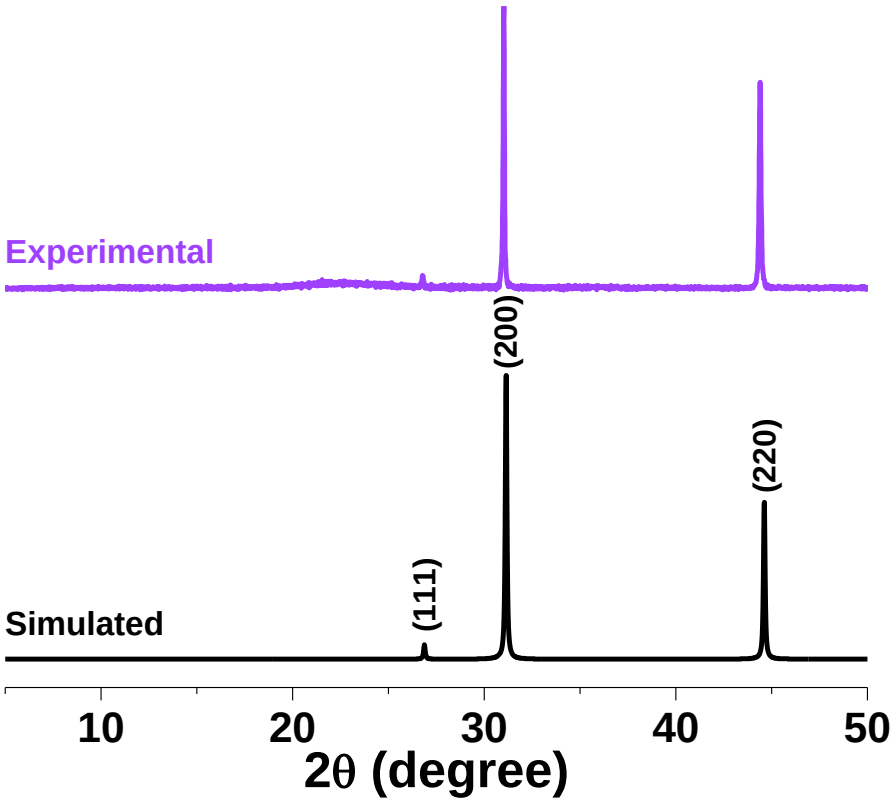

Figure S11. Comparison between the simulated and experimental PXRD patterns showing phase purity of commercial AgBr.

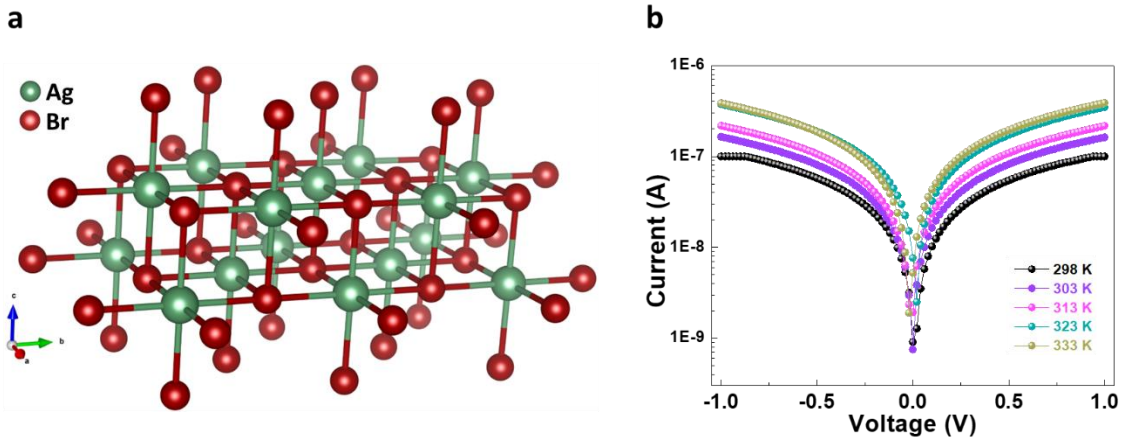

Figure S12. (a) Crystal structure of AgBr. (b) Variable temperature current-voltage (*I-V*) properties of AgBr.

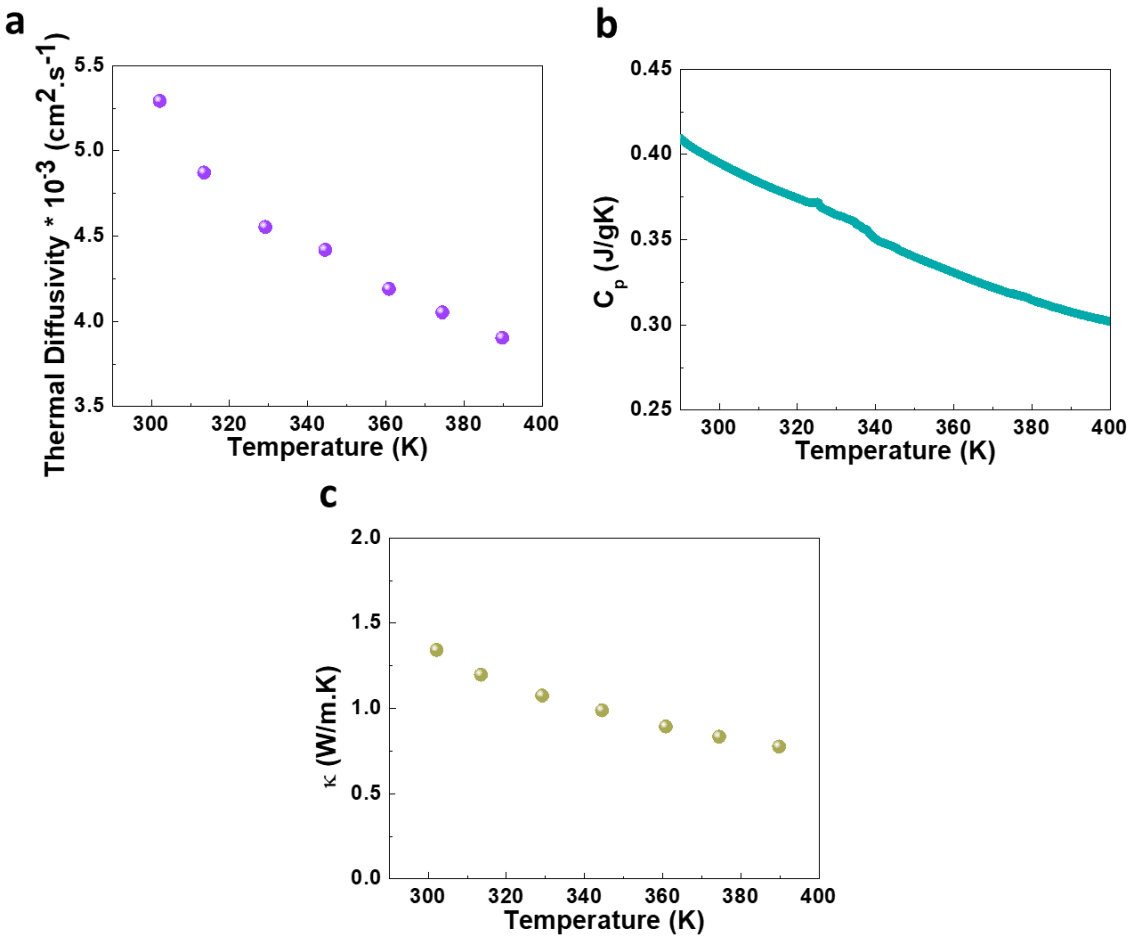

Figure S13. (a) Thermal diffusivity of AgBr as a function of temperature. (b) Heat capacity (C_p) of AgBr as a function of temperature. (c) Variable temperature thermal conductivity of AgBr.

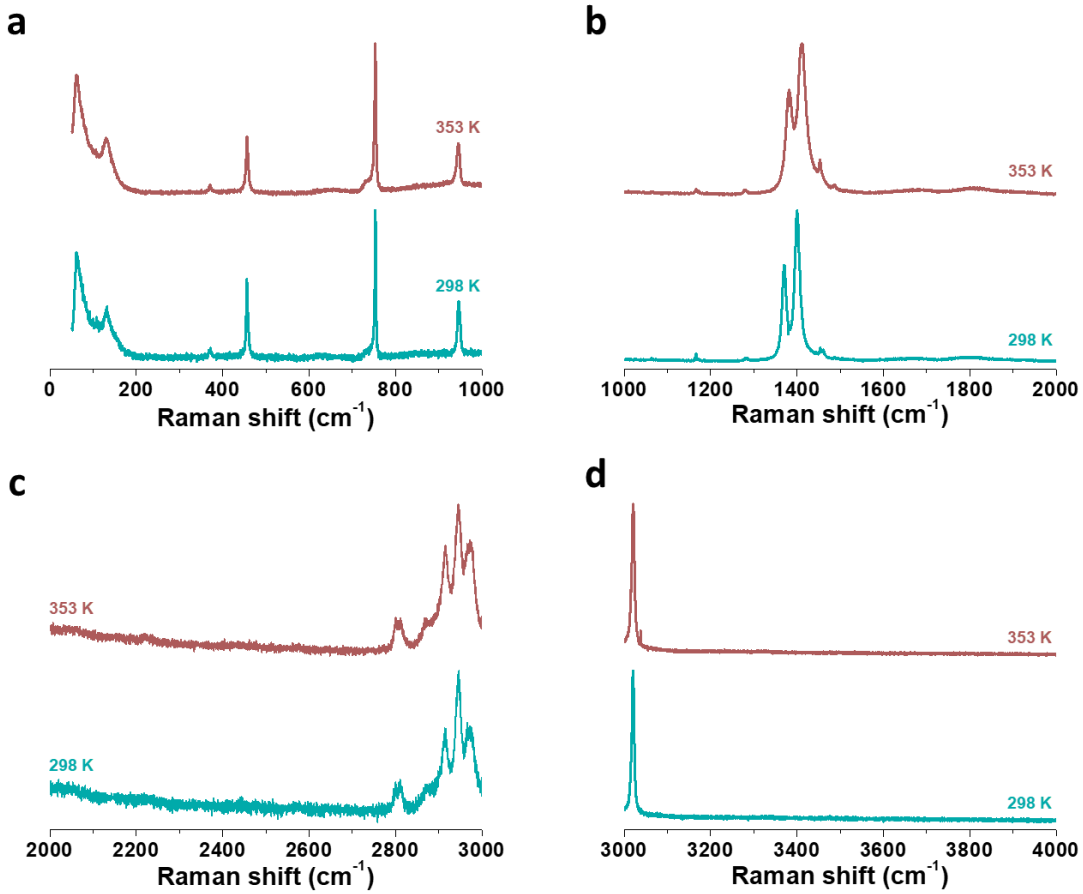

Figure S14. Zoomed-in variable temperature Raman spectra of $(TMA)AgBr_2$ in the range of (a) 0-1000 cm^{-1}, (b) 1000-2000 cm^{-1}, (c) 2000-3000 cm^{-1}, and (d) 3000-4000 cm^{-1}.

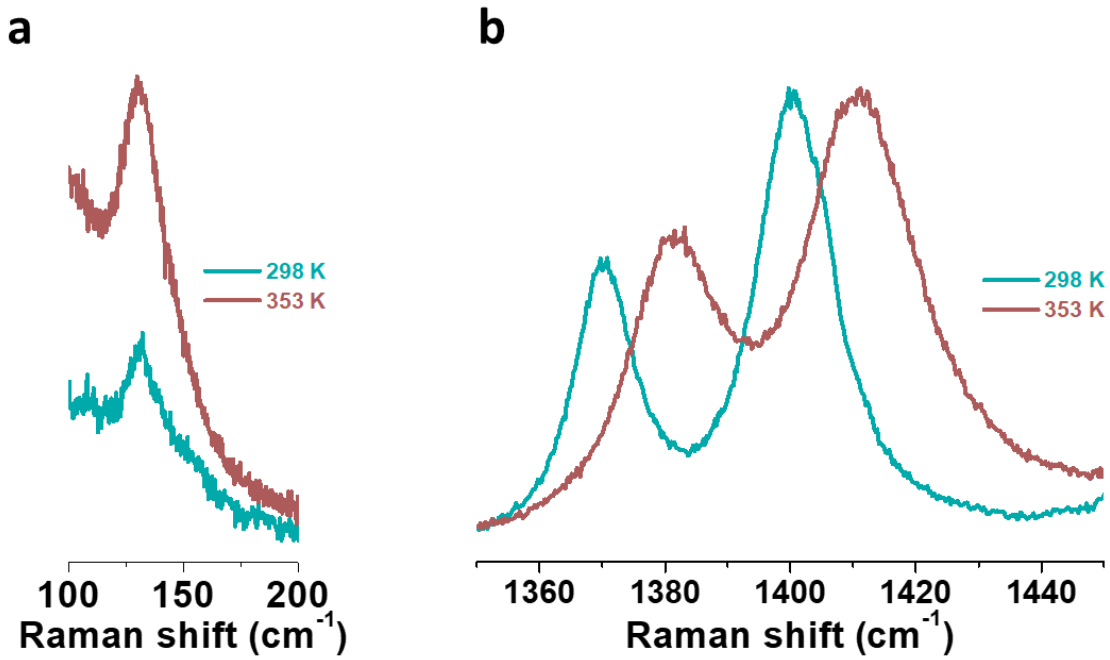

Figure S15. (a) Variable temperature Raman spectra indicative of characteristic Ag---Ag interaction. (b) Blue-shifting of Raman modes depicting change in phonon mode upon rise in temperature.

Table S7. Table of comparison of thermal conductivity of relevant reported literatures.

No.	Material	κ (W.m^{-1}.K^{-1})	References
1	$CsPbCl_3$	0.49 (RT, total)	*J. Phys. Mater.* **2020**, *3*, 024004.
2	$CsPbBr_3$	0.42 (RT, lattice)	*Proc. Natl. Acad. Sci. U. S. A.* **2017,** *114*(33), 8693-8697
3	$CsPbBr_3$	0.46 (RT, total)	*Nano Lett.* **2017**, *17*, 5734– 5739.
4	$CsPbI_3$	0.45 (RT, lattice)	*Proc. Natl. Acad. Sci. U. S. A.* **2017,** *114*(33), 8693-8697
5	$CsSnBr_3$	0.64 (RT, lattice)	*J. Am. Chem. Soc.* **2020**, 142, 9553-9563.
6	$CsSnI_3$	0.38 (RT, lattice)	*Proc. Natl. Acad. Sci. U. S. A.* **2017,** *114*(33), 8693-8697
7	$CsSnI_3$	0.6 (RT, lattice)	*J. Am. Chem. Soc.* **2020**, 142, 9553-9563.
8	$MAPbCl_3$	0.73 (RT, total)	*Nano Lett.* **2017**, *17*, 5734– 5739.
9	$MAPbCl_3$	0.50 (RT, ---)	*J. Phys. Chem. C* **2017***, 121,* 28306–28311.
10	$MAPbBr_3$	0.51 (RT, total)	*Nano Lett.* **2017**, *17*, 5734– 5739.
11	$MAPbBr_3$	0.44 (RT, ---)	*J. Phys. Chem. C* **2017***, 121,* 28306–28311.
12	$MAPbI_3$	0.5 (RT, ---)	*J. Phys. Chem. Lett.* **2014**, *5*, 2488– 2492.
13	$MAPbI_3$	0.59 (RT, lattice)	*Appl. Phys. Lett.* **2016**, *108*, 063902.
14	$MAPbI_3$	0.34 (RT, ---)	*J. Phys. Chem. C* **2017***, 121,* 28306–28311.
15	$FAPbBr_3$	0.49 (RT, total)	*Nano Lett.* **2017**, *17*, 5734– 5739.
16	$CuBiI_4$	0.38 (RT) (lattice)	*J. Am. Chem. Soc.*, **2023**, *145*, 1349-1358.
17	Cu_2Se	0.48 (1000 K, lattice)	*Nat. Mater.* **2012**, *11*, 422.
18	$CuFeS_2$	8.42 (RT, lattice)	*J. Am. Chem. Soc.* **2019**, *141 (47)*,18900−18909.
19	Ag_2Te	0.93 (RT, total)	*J. Alloys Compd.* **2005**, *393*, 299−301.
20	$AgSbSe_2$	0.42 (100 K, lattice)	*Energy Environ. Sci.* **2013**, *6*, 570–578.
21	$AgSbTe_2$	0.6 (RT, lattice)	*ACS Energy Lett.* **2021**, *6 (8)*, 2825−2837.
22	$AgBiS_2$	0.68 (RT, lattice)	*Chem. Mater.* **2019**, *31 (6)*, 2106−2113.
23	$AgBiSe_2$	0.63 (100 K, lattice)	*Energy Environ. Sci.* **2013**, *6*, 570–578.
24	$AgSnSbTe_3$	0.47 (294 K, lattice)	*Angew. Chem. Int. Ed.* **2023**, *62*, e202308515.
25	$AgPbBiSe_3$	0.5 (290 K, lattice)	*Chem. Sci.* **2019**, *10 (18)*, 4905−4913.
26	$Ag_{10}Te_4Br_3$	0.43 (390 K, total)	*Nat. Mater.* **2009**, *8(2)*, 101−108.
27	$CsAg_5Te_3$	0.18 (296 K, total)	*Angew. Chem.,Int. Ed.* **2016**, *55 (38)*, 11431−11436.
28	$AgCrSe_2$	0.46 (625 K, lattice)	*Nat. Mater.* **2018**, *17 (3)*, 226−230.

29	$Rb_4Ag_2BiBr_9$	0.1 (RT, total)	*Cryst. Growth Des.* **2022**, *22*, 1066 − 1072.
30	$(C_3H_7NH_3)_4CuInCl_8$	0.15 (RT, lattice) || to pressing	*Angew. Chem. Int. Ed.* **2024**, e202406616
31	$(TMA)AgBr_2$	0.6 (RT, total)	This Work

References

(1) Dolomanov, O. V.; Bourhis, L. J.; Gildea, R. J.; Howard, J. A. K.; Puschmann, H., OLEX2: a complete structure solution, refinement and analysis program. *J. Appl. Crystallogr.* **2009,** *42*, 339-341.
(2) Sheldrick, G., Crystal structure refinement with SHELXL. *Acta Cryst. C* **2015,** *71*, 3-8.
(3) Spek, A., Single-crystal structure validation with the program PLATON. *J. Appl. Crystallogr.* **2003,** *36*, 7-13.
(4) Hafner, J., Ab-initio simulations of materials using VASP: Density-functional theory and beyond. *J. Comput. Chem.* **2008,** *29*, 2044-2078.
(5) Anisimov, V. I.; Zaanen, J.; Andersen, O. K., Band theory and Mott insulators: Hubbard U instead of Stoner I. *Phys. Rev. B* **1991,** *44*, 943-954.